Digital Signal Processing ••• (••••) •••–•••

Contents lists available at ScienceDirect

Digital Signal Processing

www.elsevier.com/locate/dsp

Volume-based method for spectrum sensing ☆

Lei Huang [a,*], H.C. So [b], Cheng Qian [b]

[a] Department of Electronic and Information Engineering, Harbin Institute of Technology Shenzhen Graduate School, Shenzhen, China
[b] Department of Electronic Engineering, City University of Hong Kong, Hong Kong, China

ARTICLE INFO

Article history:
Available online xxxx

Keywords:
Spectrum sensing
Cognitive radio
Signal detection
Random matrix theory

ABSTRACT

It is recently shown that algorithms derived from random matrix theory (RMT) can provide superior performance for spectrum sensing, which corresponds to the task of detecting the presence of primary users in cognitive radio. The essence of the RMT-based methods is to utilize the distribution of extremal eigenvalues of the received signal sample covariance matrix (SCM), namely, the Tracy–Widom (TW) distribution. Although the TW distribution is quite useful in spectrum sensing, computationally demanding numerical evaluation is required because it does not have an explicit closed-form expression. In this paper, we devise two novel volume-based detectors by exploiting the determinant of the SCM or volume to distinguish between the signal-presence and signal-absence cases. With the use of RMT, we accurately produce the theoretical decision threshold for one of the detectors under the Gaussian noise assumption. Simulation results are included to illustrate the effectiveness of the volume-based detectors.

1. Introduction

It has been revealed in [1] that the current policies of fixed spectrum allocation do not fully utilize the available spectrum. Cognitive radio (CR) [2–12], whose main idea is to sense the spectrum over a wide range of frequency bands and exploit the temporally unoccupied bands for opportunistic wireless transmissions, is a promising paradigm to increase the spectrum usage efficiency. In a CR network, when the spectrum resources of a primary user (PU) are not occupied, a secondary user (SU) is allowed to use them. That is to say, the SU needs to reliably detect the presence of the PU. This is referred to as spectrum sensing, which can be cast as a binary hypothesis testing problem and is particularly challenging for small sample size and/or low signal-to-noise ratio (SNR) conditions.

For the scenario of signal-absence, the observed data only consist of noise and are usually assumed to be independent and identically distributed (IID). It is apparent that the energy and correlation structure of the observations differ when the PU signal is present. As a result, spectrum sensing can be achieved by making use of these dissimilarities. When the noise power is known, the energy detector (ED) [13,14] has been shown to be optimal for the IID PU signals. However, the noise power information is usually unavailable in practice and thus its estimate is used instead [15–17]. This can dramatically degrade the detection performance of the ED approach because it is quite sensitive to the noise uncertainty. As a matter of fact, the eigenvalues of the received signal sample covariance matrix (SCM) in the signal-presence situation are more spread out than those in the noise-only case, which corresponds to a scaled identity matrix in the asymptotic sense. The spread-out eigen-spectrum results from the correlation structure inherent in the covariance matrix. As a result, a number of eigenvalue-based detectors which exploit the correlation structure for spectrum sensing have been proposed in the literature [18–25]. Derived in the framework of generalized likelihood ratio test (GLRT), the arithmetic-to-geometric mean (AGM) method [18] is able to reliably identify the correlated signals embedded in the IID noise. However, the AGM algorithm has its root in the maximum likelihood (ML) theory which turns out to be inefficient when the temporal and spatial dimensions are small, that is, the theoretical decision threshold cannot be accurately determined. On the other hand, the maximum-to-minimum eigenvalue (MME) approach [19] is heuristically developed to test if the SCM corresponds to an identity matrix or its correlated alternative with the use of its maximum and minimum eigenvalues. Since not all eigenvalues are utilized, its detection performance is highly sensitive to weak correlated signals and/or small sample sizes. Moreover, computation of the theoretical threshold for the MME algorithm

☆ The work described in this paper was in part supported by a grant from the NSFC/RGC Joint Research Scheme sponsored by the Research Grants Council of Hong Kong and the National Natural Science Foundation of China (Project No.: N_CityU 104/11, 61110229/61161160564), by the National Natural Science under Grants 61222106 and 61171187 and by the Shenzhen Kongqie talent program under Grant KQC201109020061A.
* Corresponding author.
E-mail addresses: dr.lei.huang@ieee.org (L. Huang), hcso@ee.cityu.edu.hk (H.C. So), alextoqc@gmail.com (C. Qian).

http://dx.doi.org/10.1016/j.dsp.2014.02.003
1051-2004/

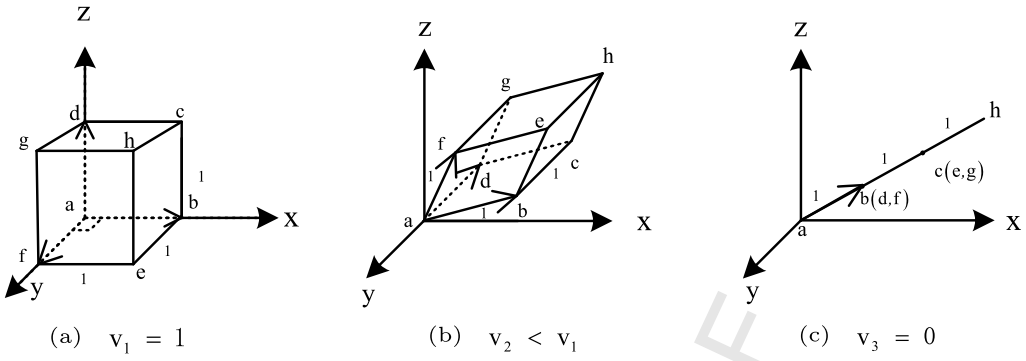

Fig. 1. Volume comparison for uncorrelated, correlated and coherent observations.

relies on the distribution of the maximum and minimum eigenvalues in the framework of random matrix theory (RMT), namely, the Tracy–Widom (TW) distribution [26]. However, there is no explicit closed-form expression for the TW distribution, indicating that an additional overhead of numerical evaluation is required. For the situation where there is only a single primary signal, an accurate variant of the GLRT has been devised for spectrum sensing in [24], which is equivalent to the signal-to-noise (mean) eigenvalue (SNE) method [21]. As discussed in [27,30], nevertheless, the number of primary signals in the sensed channel can be more than one. Under such a condition, the performance of the SNE method cannot be guaranteed. In practice, the SU receivers are usually uncalibrated, making the noises at different antennas to be non-uniform. To handle the non-uniform noise, some robust sensing approaches have been proposed, such as the GLRT test [28], independence test [29], Hadamard ratio test [27,30] and locally most powerful invariant test (LMPIT) [31]. In this work, a new philosophy for spectrum sensing is devised to accurately and robustly detect the PUs in a computationally attractive manner. The underlying idea is that the determinant of SCM or volume differs dramatically between the signal-absence and signal-presence situations.

The rest of the paper is organized as follows. The problem formulation of spectrum sensing is presented in Section 2. In Section 3, prior to deriving the volume-based detectors, the motivation is provided via geometric interpretation. Then two volume-based detectors, denoted by VD1 and VD2, are developed for spectrum sensing. With the use of RMT, the theoretical decision threshold of the VD2 is accurately determined and no numerical procedure is involved. Simulation results are included in Section 4 to evaluate the performance of the proposed detectors by comparing with the ED, AGM, MME, Hadamard ratio and SNE methods. Finally, conclusions are drawn in Section 5.

2. Problem formulation

Consider a multipath fading channel model and assume there are 1 PU and $(d-1)$ interference users with $d \geqslant 1$, and each of them is equipped with a single antenna in a CR network. To simplify the following presentation, the interference users are now counted as PUs because they occupy the same channel, that is, there are d PUs. To find a temporally unoccupied channel, a SU receiver with m antennas needs to monitor this channel. Denote the signal-absence and signal-presence hypotheses by $\mathcal{H}_0$ and $\mathcal{H}_1$, respectively. The output observations of the SU, $\boldsymbol{y}(k)$ $(k = 1, \ldots, n)$, under the binary hypotheses can be written as

$$\boldsymbol{y}(k) = \begin{cases} \boldsymbol{w}(k), & \mathcal{H}_0 \\ \boldsymbol{H}\boldsymbol{s}(k) + \boldsymbol{w}(k), & \mathcal{H}_1 \end{cases} \tag{1}$$

where n is the number of samples, $\boldsymbol{H} \in \mathbb{R}^{m\times d}$ represents the fading channels between the PUs and SU, and

$$\boldsymbol{y}(k) = \big[x_1(k), \ldots, x_m(k)\big]^T \tag{2}$$

$$\boldsymbol{s}(k) = \big[s_1(k), \ldots, s_d(k)\big]^T \tag{3}$$

$$\boldsymbol{w}(k) = \big[w_1(k), \ldots, w_m(k)\big]^T \tag{4}$$

stand for the observation, signal and noise vectors, respectively, with $(\cdot)^T$ being the transpose operator. Unless stated otherwise, the channels, primary signals and noise are considered to be real-valued[1] throughout this paper. We assume that the noises are statistically independent and satisfy $w_i(k) \sim \mathcal{N}(0, \sigma_{w_i}^2)$ $(i = 1, \ldots, m)$ where $\sigma_{w_i}^2$ is the unknown noise variance, $\sim$ represents "distributed as" and $\mathcal{N}(\mu, \Sigma)$ denotes the Gaussian distribution with mean μ and variance Σ. If $\sigma_{w_i}^2 = \sigma_w^2$ for $i = 1, \ldots, m$, the noise becomes IID (uniform); otherwise, it is the non-uniform noise due to the uncalibrated receiver [28,32]. Meanwhile, suppose that $s_i(k)$ $(i = 1, \ldots, d)$ is a random process with mean zero and unknown variance $\sigma_{s_i}^2$, which is independent of the noise. Note that the primary signal vector $\boldsymbol{s}(k)$ is unnecessarily Gaussian distributed. In order to exploit the correlation structure inherent in the observations, we employ the covariance matrix of $\boldsymbol{y}(k)$, given as

$$\boldsymbol{R} = \mathbb{E}\big[\boldsymbol{y}(k)\boldsymbol{y}^T(k)\big] \tag{5}$$

where $\mathbb{E}[\cdot]$ is the expectation operator.

3. Volume-based detector for spectrum sensing

3.1. Geometric interpretation

The determinant of $\boldsymbol{R}$ in fact is the hyper-volume of the geometry determined by the row vectors of $\boldsymbol{R}$. As an example, let us consider the scenario of three receiving antennas where the observed data with zero mean and unity variance may be independent, correlated or coherent. This means that the corresponding covariance matrices are the 3×3 identity matrix, full-rank non-identity matrix and rank-one arbitrary matrix. The geometries, namely, cube, parallelepiped and line, formed by the row vectors of the matrices are depicted in Fig. 1, where all edges of the geometries are assumed to be unity such that $\|\boldsymbol{R}(i,:)\| = 1$ with $\boldsymbol{R}(i,:)$ being the i-th row of $\boldsymbol{R}$ and $\|\cdot\|$ being the Euclidean norm. Here, the volumes of the cube, parallelepiped and line, are denoted by v_1, v_2 and v_3, respectively. The cube corresponds to the case of signal-absence whereas the other two geometries are referring to the cases of signal-presence. For the signal-absence situation, the covariance matrix is a 3×3 identity matrix, i.e., $\boldsymbol{R} = \boldsymbol{I}_3$, whose rows determine the coordinates of the points b, f and d in Fig. 1(a), that is, $(x_b, y_b, z_b) = (1, 0, 0)$, $(x_f, y_f, z_f) = (0, 1, 0)$, $(x_d, y_d, z_d) = (0, 0, 1)$. Consequently, we obtain $v_1 = 1$. For the

[1] The proposed methods can be readily applied to the complex-valued case by transforming the complex observation to its real counterpart, see [33] for example.

signal-presence scenarios, however, the structure of diagonal matrix is destroyed, leading to significant volume reduction, as indicated in Fig. 1(b) and (c). Consequently, the volume is able to differentiate the PUs from the background noise, motivating us to develop a new methodology for accurate spectrum sensing.

3.2. Derivation

Let us begin with the case of signal-absence. In this case, the elements of $\boldsymbol{y}(k)$, that is, $y_i(k)$, $k = 1, \ldots, n$, $i = 1, \ldots, m$, are the independent observations. To exploit the correlation structure for spectrum sensing in practice, we compute the SCM rather than the population covariance matrix $\boldsymbol{R}$, which is given by

$$\boldsymbol{S} = \frac{1}{n}\sum_{k=1}^{n} \boldsymbol{y}(k)\boldsymbol{y}^T(k). \tag{6}$$

Meanwhile, the edge lengths associated with the row vectors of the SCM are calculated as $\delta_i = \|\boldsymbol{S}(i,:)\|$ $(i = 1, \ldots, m)$. By setting $\boldsymbol{D} = \mathrm{diag}(\delta_1, \ldots, \delta_m)$, we are able to obtain the volume of the geometry with unity edge, that is, $\det[\boldsymbol{D}^{-1}\boldsymbol{S}]$. Taking the logarithm, we have

$$\xi_1 \triangleq \log\det\big[\boldsymbol{D}^{-1}\boldsymbol{S}\big]. \tag{7}$$

For the scenario of signal-absence, $\boldsymbol{D}^{-1}\boldsymbol{S}$ asymptotically approaches the identity matrix as the number of samples tends to infinity, leading to the volume of one. For the situation of signal-presence, however, the correlation between the rows of $\boldsymbol{D}^{-1}\boldsymbol{S}$ results in considerable reduction of volume, providing a good indication for the primary signals. Therefore, compared with a predetermined threshold γ_1, the statistic ξ_1 is able to yield correct detection of the PUs. That is

$$\xi_1 \underset{\mathcal{H}_1}{\overset{\mathcal{H}_0}{\gtrless}} \gamma_1. \tag{8}$$

However, it is very hard to determine the theoretical threshold for ξ_1 as the distribution of $\det[\boldsymbol{D}^{-1}\boldsymbol{S}]$ is unknown. To alleviate the difficulty, we assume that the noise is IID and derive an equivalent statistic. It is easy to obtain

$$\begin{aligned}\log\det\big[n\boldsymbol{D}^{-1}\boldsymbol{S}\big] &= \log\det\left[\hat{\sigma}_w^2\boldsymbol{D}^{-1}\times\frac{\sigma_w^2}{\hat{\sigma}_w^2}\times\frac{n\boldsymbol{S}}{\sigma_w^2}\right]\\ &= \log\det\left[\frac{n\boldsymbol{S}}{\sigma_w^2}\right] - \log\det\left[\frac{\boldsymbol{D}}{\hat{\sigma}_w^2}\right]\\ &\quad - m\log\left(\frac{\hat{\sigma}_w^2}{\sigma_w^2}\right)\end{aligned} \tag{9}$$

where $\hat{\sigma}_w^2$ is the estimated noise variance calculated by $\hat{\sigma}_w^2 = \mathrm{var}(\boldsymbol{Y}(:))$ where $\boldsymbol{Y}(:)$ results from the vectorization of $\boldsymbol{Y} \triangleq [\boldsymbol{y}(1), \ldots, \boldsymbol{y}(n)]$. Consequently, we get

$$\begin{aligned}\xi_2 &\triangleq \log\det\left[\frac{n\boldsymbol{S}}{\sigma_w^2}\right]\\ &= \log\det\big[n\boldsymbol{D}^{-1}\boldsymbol{S}\big] + \log\det\left[\frac{\boldsymbol{D}}{\hat{\sigma}_w^2}\right] + m\log\left(\frac{\hat{\sigma}_w^2}{\sigma_w^2}\right).\end{aligned} \tag{10}$$

It should be pointed out that the noise variance can be accurately estimated by $\hat{\sigma}_w^2 = \mathrm{var}(\boldsymbol{Y}(:))$ for the noise-only hypothesis $\mathcal{H}_0$, enabling us to accurately determine the threshold for ξ_2 provided that the last term on the right hand side (RHS) of (10) can be fixed. For the signal-presence hypothesis $\mathcal{H}_1$, however, the noise variance cannot be correctly estimated, making $\xi_2|\mathcal{H}_1$ to have a different behavior from $\xi_2|\mathcal{H}_0$ and thereby enabling us to correctly detect the presence of the primary signals. Note that the last term on the RHS of (10) cannot be calculated from $\boldsymbol{y}(k)$ as it requires the true noise variance σ_w^2. To circumvent this problem, we derive an estimate to approximate it. To this end, setting

$$\hat{b} = m\log\left(\frac{\hat{\sigma}_w^2}{\sigma_w^2}\right) \tag{11}$$

and noticing that the noise variance can be accurately calculated from the $mn \times 1$ observations $\boldsymbol{Y}(:)$ in the noise-only case, we utilize $\mathbb{E}[\hat{b}]$ to approximate $\hat{b}$, or

$$\mathbb{E}[\hat{b}] \approx \hat{b}. \tag{12}$$

This approximation is valid because $\hat{b}$ is much smaller than the other two terms in (10). On the other hand, it follows from [34] that

$$\frac{\hat{\sigma}_w^2}{\sigma_w^2} \triangleq \frac{1}{mn}u \sim \frac{1}{mn}\chi^2(mn) \tag{13}$$

where $u \sim \chi^2(mn)$ with $\chi^2(mn)$ being the chi-squared distribution with mn degrees of freedom. Substituting (13) into (11) and taking the expectation yield

$$\mathbb{E}[\hat{b}] = m\mathbb{E}\big[\log(\hat{\sigma}_w^2/\sigma_w^2)\big] = m\left(\log\frac{1}{mn} + \mathbb{E}[\log u]\right). \tag{14}$$

To proceed, we need the following lemma [35]

Lemma 1. *If $u \sim \chi^2(J)$, then*

$$\mathbb{E}[\log u] = \log(J) - \frac{1}{J} - \frac{1}{3J^2} + \frac{2}{15J^4} + \mathcal{O}\big(J^{-6}\big). \tag{15}$$

Proof. The proof of Lemma 1 is given in [35]. □

Consequently, substituting (15) into (14) gives

$$\begin{aligned}\mathbb{E}[\hat{b}] &= -m\left(\frac{1}{mn} + \frac{1}{3(mn)^2} - \frac{2}{15(mn)^4} - \mathcal{O}\big((mn)^{-6}\big)\right)\\ &\approx -m\left(\frac{1}{mn} + \frac{1}{3(mn)^2} - \frac{2}{15(mn)^4}\right) \triangleq b.\end{aligned} \tag{16}$$

It follows from (12) and (16) that $\hat{b}$ can be approximated by b. As a result, the test statistic ξ_2 in (10) can be reexpressed as

$$\xi_2 \approx \log\det\big[n\boldsymbol{D}^{-1}\boldsymbol{S}\big] + \log\det\left[\frac{\boldsymbol{D}}{\hat{\sigma}_w^2}\right] + b. \tag{17}$$

It should be pointed out that, although ξ_2 relies on the estimated noise variance $\hat{\sigma}_w^2$ but is insensitive to the uncertainty in the latter because the first term on the RHS is much larger than the other two terms. This can also be verified by the simulation results in Section 4. For the case of signal-presence, however, the statistic variable must have a different behavior due to the fact that the volumes in both hypotheses are different. As a result, for a given threshold γ_2, the decision problem can be stated as

$$\xi_2 \underset{\mathcal{H}_1}{\overset{\mathcal{H}_0}{\gtrless}} \gamma_2. \tag{18}$$

The proposed volume-based algorithms for spectrum sensing, denoted by VD1 and VD2 corresponding to the test statistics ξ_1 and ξ_2, are summarized in Tables 1 and 2, respectively. The threshold of the VD1 is determined by Monte Carlo simulation while that of the VD2 can be obtained by either Monte Carlo simulation or asymptotically theoretical calculation which will be elaborated in the next subsection.

Table 1
Summary of VD1.

Step 1:	Compute the SCM by $\boldsymbol{S}=(1/n)\boldsymbol{Y}\boldsymbol{Y}^T$ with $\boldsymbol{Y}\triangleq[\boldsymbol{y}(1),\ldots,\boldsymbol{y}(n)]$ and their edges by $\delta_i=\|\boldsymbol{S}(i,:)\|$ for $i=1,\ldots,m$.
Step 2:	Form the test statistic as $\xi_1=\log\det(\boldsymbol{D}^{-1}\boldsymbol{S})$ with $\boldsymbol{D}=\mathrm{diag}(\delta_1,\ldots,\delta_m)$.
Step 3:	Compare ξ_1 with the predetermined threshold γ_1. If $\xi_1<\gamma_1$, the primary signals are present; otherwise, the signals do not exist.

Table 2
Summary of VD2.

Step 1:	Calculate the noise variance $\hat{\sigma}_w^2$ from the observations $\boldsymbol{Y}\triangleq[\boldsymbol{y}(1),\ldots,\boldsymbol{y}(n)]$, i.e., $\hat{\sigma}_w^2=\mathrm{var}(\boldsymbol{Y}(:))$.
Step 2:	Compute the SCM via $\boldsymbol{S}=(1/n)\boldsymbol{Y}\boldsymbol{Y}^T$ and their edges by $\delta_i=\|\boldsymbol{S}(i,:)\|$ for $i=1,\ldots,m$.
Step 3:	Calculate $\hat{b}$ via (16) and form $\boldsymbol{D}=\mathrm{diag}(\delta_1,\ldots,\delta_m)$.
Step 4:	Establish the test statistic of (17) and compare it with the predetermined threshold γ_2. If $\xi_2<\gamma_2$, the primary signals are present; otherwise, the signals do not exist.

3.3. Asymptotic theoretical threshold for VD2

If the probability density functions (PDFs) of ξ_2 under hypotheses $\mathcal{H}_0$ and $\mathcal{H}_1$, denoted as $f_0(t)$ and $f_1(t)$, are known, it follows from (18) that the false alarm probability (P_{fa}) and detection probability (P_{d}) can be calculated as

$$P_{\mathrm{fa}}=\mathrm{Prob}(\xi_2<\gamma_2\mid\mathcal{H}_0)=\int_{-\infty}^{\gamma_2}f_0(t)\,dt \tag{19}$$

$$P_{\mathrm{d}}=\mathrm{Prob}(\xi_2<\gamma_2\mid\mathcal{H}_1)=\int_{-\infty}^{\gamma_2}f_1(t)\,dt. \tag{20}$$

As a result, the threshold γ_2 may be derived from the P_{fa} or P_{d} provided that $f_0(t)$ or $f_1(t)$ is given. Usually, it is quite hard to determine $f_1(t)$ as the statistic ξ_2 relies on the correlation of the received signals, which in fact varies under different environments. On the contrary, it is easy to determine $f_0(t)$ by means of the following theorem due to Jonsson [36].

Theorem 1. *Let the observation data $y_i(k)$, $i=1,\ldots,m$, $k=1,\ldots,n$, be independent normal variables with zero mean and unity variance. If $m,n\to\infty$ and $m/n\to c\in(0,1)$ with c being a fixed number, then the test statistic ξ_2 is Gaussian distributed, that is,*

$$\xi_2=\log\det\left[\frac{n\boldsymbol{S}}{\sigma_w^2}\right]\sim\mathcal{N}\left(\mu_\xi,\sigma_\xi^2\right) \tag{21}$$

where $\boldsymbol{S}$ is the SCM given in (6), $\sigma_\xi^2=-2\log(1-c)$ and $\mu_\xi=\log(n-1)_m$ with $(n-1)_m=(n-1)(n-2)\cdots(n-m)$.

Proof. The proof of Theorem 1 is provided in [36]. □

As $\xi_2\sim\mathcal{N}(\mu_\xi,\sigma_\xi^2)$ under the noise-only environment, it follows from (19) that

$$P_{\mathrm{fa}}=1-\int_{\frac{\gamma_2-\mu_\xi}{\sigma_\xi}}^{\infty}g(t)\,dt=1-Q\left(\frac{\gamma_2-\mu_\xi}{\sigma_\xi}\right) \tag{22}$$

where $Q(x)=\int_x^\infty g(t)\,dt$ with $g(t)=1/\sqrt{2\pi}\exp(-t^2/2)$. Thus, for a given false alarm level $\varepsilon=P_{\mathrm{fa}}$, the decision threshold γ_2 can be determined as

$$\gamma_2=\sigma_\xi Q^{-1}(1-\varepsilon)+\mu_\xi \tag{23}$$

Table 3
Expression for theoretical threshold.

Method	Test Statistic	Threshold (γ)
AGM	$n\log[\frac{(1/m)\sum_{i=1}^m\ell_i}{(\prod_{i=1}^m\ell_i)^{1/m}}]^m$ [18]	$2\bar{\Gamma}^{-1}(1-\varepsilon,(m^2+m)/2-1)$
MME	ℓ_1/ℓ_m [19]	$\frac{(\sqrt{n}+\sqrt{m})^2}{(\sqrt{n}-\sqrt{m})^2}\times(1+\frac{(\sqrt{n}+\sqrt{m})^{-2/3}}{(mn)^{1/6}}T_2^{-1}(1-\varepsilon))$
SNE	$\frac{\ell_1}{\frac{1}{m-2}\sum_{i=2}^m\ell_i}$ [24]	$\frac{(1+\sqrt{m/n})^2}{m-1}+\frac{(\sqrt{m}+\sqrt{n})^{4/3}}{n(m-1)(\sqrt{mn})^{1/3}}T_2^{-1}(1-\varepsilon)$
ED(σ_w^2)	$\mathrm{tr}[\hat{\boldsymbol{R}}]/\sigma_w^2$ [38]	$2\bar{\Gamma}^{-1}(1-\varepsilon,mn)$
ED($\hat{\sigma}_w^2$)	$\mathrm{tr}[\hat{\boldsymbol{R}}]/\hat{\sigma}_w^2$ [38]	$F^{-1}(1-\varepsilon,mn,L)$

where $Q^{-1}(x)$ is the inverse function of $Q(x)$. As suggested by Bai and Silverstein [37], it is reasonable to replace $c=\lim_{m,n\to\infty}m/n$ by m/n in the calculation of γ_2.

4. Simulation results

4.1. Accuracy of theoretical decision threshold

Let us first evaluate the accuracy of the theoretical decision thresholds. Table 3 gives the formulae for computing the theoretical thresholds of the AGM [18], MME [19], SNE [24], ED(σ_w^2) [13] and ED($\hat{\sigma}_w^2$) [38] methods, where the ED(σ_w^2) and ED($\hat{\sigma}_w^2$) stand for the ED methods using the true and estimated noise variances, respectively. Meanwhile, the test statistics associated with the methods are provided as well. Herein, $\bar{\Gamma}^{-1}(\cdot)$ is the inverse of the incomplete gamma function evaluated by the MATLAB built-in function `gammaincinv`$(\cdot,\cdot)$, $T_1^{-1}(\cdot)$ is the inverse of the cumulative distribution function (CDF) of the TW distribution of order one[2] [26] and $F^{-1}(\cdot,\cdot,\cdot)$ is the inverse of the CDF of the F distribution [40]. Since a number of the state-of-the-art methods have been considered, some classical detectors, such as Roy's largest root test and Wilks' likelihood ratio test [41], are not included.

To accurately determine the simulated threshold, we have carried out 50,000 independent Monte Carlo trials in the absence of PUs and select the decision thresholds for the investigated methods according to the same given false alarm level. The numerical results are tabulated in Table 4 for $m=6$ and $n=12$, where the relative error is calculated as Error $\triangleq(|\gamma_{the}-\gamma_{sim}|)/\gamma_{sim}\times100\%$ with γ_{the} and γ_{sim} being the theoretical and simulated thresholds, respectively. The noise is the IID Gaussian process with zero mean and unknown variance σ_w^2. Furthermore, we assume that there are L signal-free samples available for the noise variance estimation, enabling the ED($\hat{\sigma}_w^2$) method to work properly. It is seen that the error of the VD2 method is more close to that of the ED(σ_w^2) algorithm than other algorithms. In fact, the ED(σ_w^2) method cannot be employed for spectrum sensing as the true noise variance is unknown to the receiver in practice. Therefore, it is used herein as a benchmark. Table 4 indicates that the theoretical threshold of the ED($\hat{\sigma}_w^2$) can be accurately determined by the F distribution, which is also pointed out in [38,39]. Table 5 illustrates the accuracy of the studied methods in theoretical threshold computation for $n=100$. We observe from Table 5 that, in such a large sample situation, the VD2 method yields the similar accuracy as the AGM detector, but is still superior to the MME and SNE schemes. It is easy to interpret this result. Although the theoretical thresholds of the MME and SNE approaches are determined in the framework of RMT, the former roughly replaces the smallest sample eigenvalue ℓ_m with its limit $\sigma_w^2(1-\sqrt{m/n})^2$ to determine its theoretical threshold, thereby introducing uncertainty whereas the latter re-

[2] The table for calculating the CDF of the TW distribution is available at http://math.arizona.edu/~momar/research.htm. Note that a more accurate threshold calculation for the MME method is provided in [20] but of no closed-form expression for the general case and thereby ignored here.

Table 4
Threshold comparison between theoretical calculation and numerical simulation for various methods with parameter setting: $m = 6$, $n = 12$ and $L = 12$.

Algorithm	VD2	AGM	MME	SNE	ED(σ_w^2)	ED($\hat{\sigma}_w^2$)	P_{fa}
Theoretical γ	9.0763	45.3147	50.6249	0.6701	1.5949	5.7064	10^{-3}
Simulated γ	9.3759	57.7958	130.0793	1.3088	1.5889	5.4770	10^{-3}
Errors (%)	3.1947	21.5952	61.0815	48.7962	0.3784	4.1872	10^{-3}
Theoretical γ	9.9758	37.5662	44.2586	0.6694	1.4280	3.5071	10^{-2}
Simulated γ	10.3467	47.8124	66.9504	1.0616	1.4273	3.3478	10^{-2}
Errors (%)	3.5853	21.4299	33.8935	36.9498	0.0494	4.7565	10^{-2}
Theoretical γ	11.2059	28.4120	36.2624	0.6614	1.2187	1.9507	10^{-1}
Simulated γ	11.4633	35.8901	29.8481	0.8069	1.2181	1.8662	10^{-1}
Errors (%)	2.2451	20.8362	21.4900	18.0315	0.0428	4.5291	10^{-1}

Table 5
Threshold comparison between theoretical calculation and numerical simulation for various methods with parameter setting: $m = 6$, $n = 100$ and $L = 100$.

Algorithm	VD2	AGM	MME	SNE	ED(σ_w^2)	ED($\hat{\sigma}_w^2$)	P_{fa}
Theoretical γ	26.3292	45.3147	3.2885	0.3298	1.1880	1.6621	10^{-3}
Simulated γ	27.1541	46.6781	3.3657	0.4068	1.1853	1.5724	10^{-3}
Errors (%)	3.0376	2.9207	2.2944	18.9192	0.2210	5.7101	10^{-3}
Theoretical γ	26.5980	37.5662	3.0707	0.3297	1.1392	1.4594	10^{-2}
Simulated γ	27.2356	38.1591	2.9870	0.3766	1.1394	1.3874	10^{-2}
Errors (%)	2.3412	1.5537	2.7996	12.4709	0.0190	5.1915	10^{-2}
Theoretical γ	26.9655	28.4120	2.7971	0.3279	1.0747	1.2295	10^{-1}
Simulated γ	27.3271	29.0852	2.5542	0.3398	1.0749	1.1943	10^{-1}
Errors (%)	1.3233	2.3147	9.5078	3.5257	0.0250	2.9454	10^{-1}

lies on the approximation $(1/(m-1))\sum_{i=2}^{m}\ell_i) \approx \sigma_w^2$ which turns out to be inaccurate particularly when m and n are small.

4.2. Detection performance

In this subsection, the detection performance of the proposed algorithms is evaluated by utilizing the *simulated* thresholds. For the purpose of comparison, the results of the AGM, MME, Hadamard ratio [30], SNE, ED(σ_w^2) and ED($\hat{\sigma}_w^2$) methods are presented as well. The *simulated* thresholds of the VD1 and Hadamard ratio schemes are also obtained from 50,000 independent Monte Carlo trials whereas the *simulated* thresholds of the other schemes are given in Tables 4 and 5. Throughout this paper, the channels $\boldsymbol{H}$ are randomly drawn from a distribution and then fixed during the sensing period at each run. For simplicity, the columns of $\boldsymbol{H}$ are normalized to unity so that the SNR can be defined as $10\log_{10}\frac{\text{tr}[\boldsymbol{R}_s]/d}{\text{tr}[\boldsymbol{R}_w]/m}$ with $\boldsymbol{R}_s = \mathbb{E}[\boldsymbol{s}(k)\boldsymbol{s}^T(k)]$ and $\boldsymbol{R}_w = \mathbb{E}[\boldsymbol{w}(k)\boldsymbol{w}^T(k)]$. In this experiment, the channel is generated from a zero-mean Gaussian distribution and the detection probability is calculated using 5,000 independent trials.

Fig. 2(a) depicts the detection probability versus SNR for small samples and a single primary signal. It is seen that, by using the correlation structure of the received signal, the proposed methods outperform the MME, Hadamard ratio and ED($\hat{\sigma}_w^2$) algorithms, but are a little bit inferior to the AGM method in terms of detection probability for the small sample setting. On the other hand, as the SNE approach utilizes the information of primary source number, that is, $d = 1$ is *a priori* known to the receiver, it is superior to the blind schemes which do not employ the knowledge of d and σ_w^2. Nevertheless, although the AGM and SNE algorithms are able to provide higher detection accuracy than the VD2 method in this case, the latter is able to yield much more accurate theoretical threshold than the former, as has been verified by Table 4. When the number of primary signals is larger than one, say, $d = 3$, the SNE method suffers from performance degradation, as is illustrated in Fig. 2(b). Here, the primary signals are assumed to be uncorrelated and of equal powers. On the other hand, as the sample size becomes sufficiently large, say, $n = 100$, the performance of the VD2 detector is very close to that of the AGM scheme, and better than that of the VD1, Hadamard ratio, SNE and MME approaches. This is demonstrated in Fig. 2(c). Recall that the AGM approach is actually the variant of the GLRT, which becomes optimal in the sense of ML estimation for sufficiently large samples. However, as the SNE method assumes that the number of PUs is one, its detection accuracy is degraded for $d = 3$. Since the Hadamard ratio and VD1 detectors ignore the fact that the noise is IID, their performance is also somewhat inferior to the AGM and VD2 schemes. The MME method only employs the maximum and minimum sample eigenvalues for detection, having not utilized the information of any other sample eigenvalues, its detection performance is inferior to that of the other approaches.

4.3. Extension to complex-valued case

For the noise-only hypothesis, the independent complex Gaussian observations $\boldsymbol{x}(k)$ can be easily expressed as $\boldsymbol{x}(k) = \boldsymbol{x}_R(k) + j\boldsymbol{x}_I(k)$ with $\boldsymbol{x}_R(k)$ and $\boldsymbol{x}_I(k)$ being the real and imaginary parts of $\boldsymbol{x}(k)$ and $j = \sqrt{-1}$. As $\boldsymbol{x}_R(k)$ is uncorrelated with $\boldsymbol{x}_I(k)$, we have $\mathbb{E}[\boldsymbol{x}(k)\boldsymbol{x}^H(k)] = \mathbb{E}[\boldsymbol{x}_R(k)\boldsymbol{x}_R^T(k)] + \mathbb{E}[\boldsymbol{x}_I(k)\boldsymbol{x}_I^T(k)] = \mathbb{E}[\boldsymbol{y}(k)\boldsymbol{y}^T(k)]$ where

$$\boldsymbol{y}(k) \triangleq \big[\boldsymbol{x}_R(k), \boldsymbol{x}_I(k)\big]. \tag{24}$$

Note that the method in [33] may also be employed to transform the complex observations to its real counterpart. However, it can lead to a singular covariance matrix for $n < 2m$. With this transformation, it is quite straightforward to extend the proposed methods to the complex-valued case. For the purpose of fair comparison, the *simulated* thresholds of all the algorithms are numerically computed from 50,000 independent Monte Carlo trials.

The primary signals, $s_i(k)$ $(i = 1, \ldots, d)$, are assumed to be QPSK modulated, which are the IID random symbols taking values $\pm\sqrt{2}/2 \pm j\sqrt{2}/2$ with equal probabilities [42,43]. The MIMO Rayleigh-fading channel has been well studied in the literature,

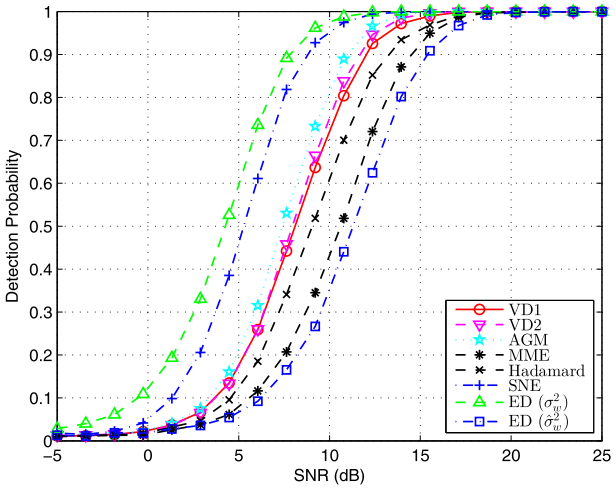

(a) $d = 1$, $n = 12$ and $L = 12$.

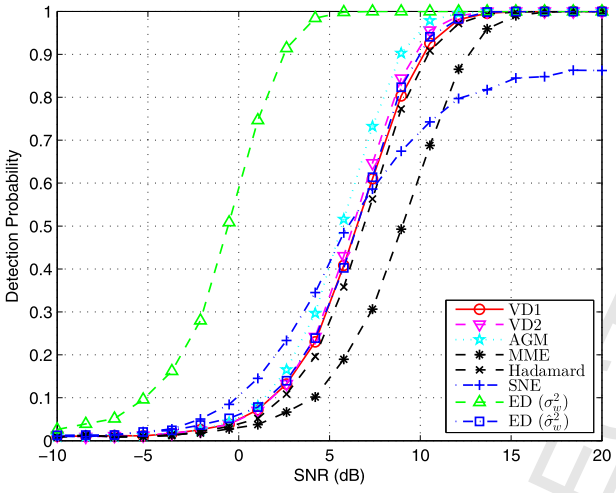

(b) $d = 3$, $\sigma_{s_1}^2 = \sigma_{s_2}^2 = \sigma_{s_3}^2$, $n = 12$ and $L = 12$.

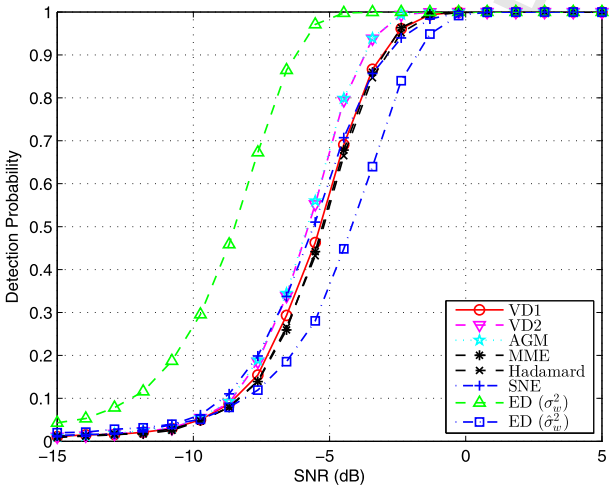

(c) $d = 3$, $n = 100$ and $L = 100$.

Fig. 2. Detection probability versus SNR for real Gaussian signals. $m = 6$ and $P_{\text{fa}} = 10^{-2}$.

such as [44–46]. It is shown in [45] that, in the Rayleigh-fading situation, the columns of the channel matrix $\boldsymbol{H}$ are complex Gaussian distributed with mean zero and covariance matrix $\boldsymbol{\Sigma}$ due to the correlation between the signals at the receiving antennas which cannot be sufficiently spaced for physical size constraints. As is indicated in [44–46], the correlated MIMO Rayleigh-fading channel model is able to precisely describe the practical channels. The (k, ℓ)-th entry of $\boldsymbol{\Sigma}$ is determined as [40, (27)]

$$\Sigma_{k\ell} = \frac{\mathcal{I}_0(\sqrt{\kappa^2 - 4\pi^2 d_{k\ell}^2 + j4\pi\kappa \sin(\mu) d_{k\ell}})}{\mathcal{I}_0(\kappa)}, \quad (k, \ell = 1, \ldots, m) \tag{25}$$

where κ controls the width of the angles-of-arrival (AOAs) of the primary signals impinging upon the antennas of the SU, which varies from 0 (isotropic scattering) up to ∞ (extremely non-isotropic scattering), $\mu \in [-\pi, \pi)$ stands for the mean direction of the AOAs, $d_{k\ell}$ is the distance, which is normalized with respect to the wavelength λ, between the k-th and ℓ-th antennas of the SU, and $\mathcal{I}_0(\cdot)$ stands for the zero-order modified Bessel function. In this simulation, we set $\kappa = 80$ and $\mu = \pi/2$, and assume that the antennas of the SU has the linear uniform array structure with the inter-element distance being $\lambda/2$. Consequently, the normalized distance between the adjacent antennas is 0.5.

The detection probabilities versus SNR for the QPSK signal in the Rayleigh-fading channel are shown in Fig. 3. For the case of multiple PUs in this sensed channel, we assume that the primary signals are uncorrelated and with equal powers. We observe from Fig. 3(a)–(b) that, for the small sample case, the VD1 and VD2 schemes are more close to the ED(σ_w^2) method than other algorithms except the SNE approach in terms of detection probability. In other words, they outperform the AGM and Hadamard ratio schemes and are significantly superior to the MME and ED($\hat{\sigma}_w^2$) algorithms at small samples. Moreover, the VD1 method is superior to the VD2 scheme. It is seen from Fig. 3(c) that, when the number of samples becomes large enough, the VD1 algorithm surpasses other algorithms, including the knowledge-based ED(σ_w^2) and SNE algorithms.

Let us now study the behaviors of various detectors in uncalibrated receiver. To focus on the effect of non-uniform noise, we only consider a single PU whose waveform is the QPSK signal. The receiver operating characteristic (ROC) curves for various detectors are plotted in Fig. 4(a) for the IID (uniform) noise whereas in Fig. 4(b) for the non-uniform noise, where the number of antennas is 4, the number of samples is 30 and the SNR equals -5 dB. Meanwhile, for the non-uniform noise, the noise powers at the four antennas are given as $[0, 1.7, -0.7, -2]$ dB. It is seen from Fig. 4(a) that the VD1 approach is more close to the benchmark than other algorithms, followed by the SNE and then by the VD2. As the Hadamard ratio detector essentially ignores the fact that the noises are IID, it is inferior to the VD1, SNE and VD2 schemes. However, it still suppresses the AGM, MME and ED($\hat{\sigma}_w^2$). In the situation of non-uniform noise, the Hadamard ratio method significantly outperforms the non-robust detectors, such as the VD2, AGM, MME, SNE, and ED($\hat{\sigma}_w^2$) approaches. Nevertheless, it is inferior to the VD1 algorithm which is as good as the benchmark, as depicted in Fig. 4(b). That is to say, only the VD1 and Hadamard ratio schemes are robust against the non-uniform noise, and the former outperforms the latter in accuracy. It should be pointed out herein that, compared with the Hadamard ratio approach, the proposed VD1 detector requires the additional constraint that the edges of the geometry formed by the SCM are normalized to unity. Without this constraint, the edges of the geometry in the Hadamard ratio approach are larger than one in the presence of PUs, which actually increases the volume. As a result, the eventual reduction in volume due to the correlation structure in the Hadamard ratio method is not so significant as that in the VD1 algorithm. This is why the VD1 approach is superior to the Hadamard ratio method in detection performance.

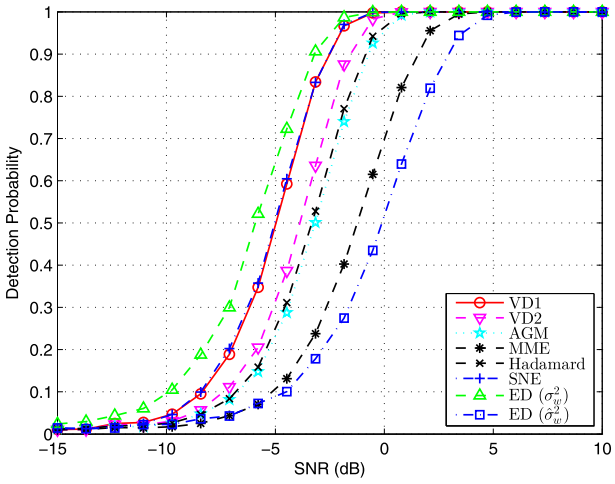

(a) $d = 1$, $n = 12$ and $L = 12$.

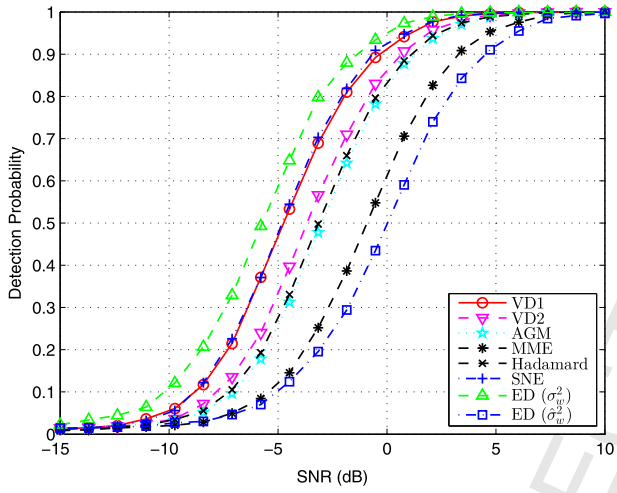

(b) $d = 3$, $n = 12$ and $L = 12$.

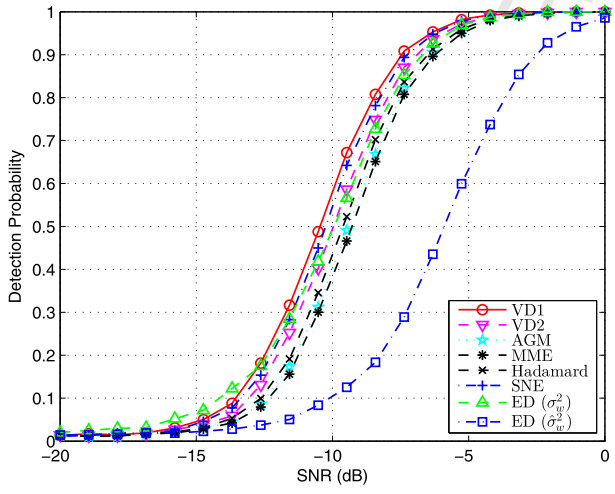

(c) $d = 3$, $n = 100$ and $L = 100$.

Fig. 3. Detection probability versus SNR for QPSK signals in Rayleigh-fading channel. $m = 6$ and $P_{\text{fa}} = 10^{-2}$.

The empirical results for another parameter setting are plotted in Fig. 5, where the number of antennas is 6, the number of samples is 100 while the SNR is −10 dB. We observe from Fig. 5(a) that, for the uniform noise, the VD1 algorithm performs the best, followed by the SNE, ED(σ_w^2) and VD2 algorithms which are very

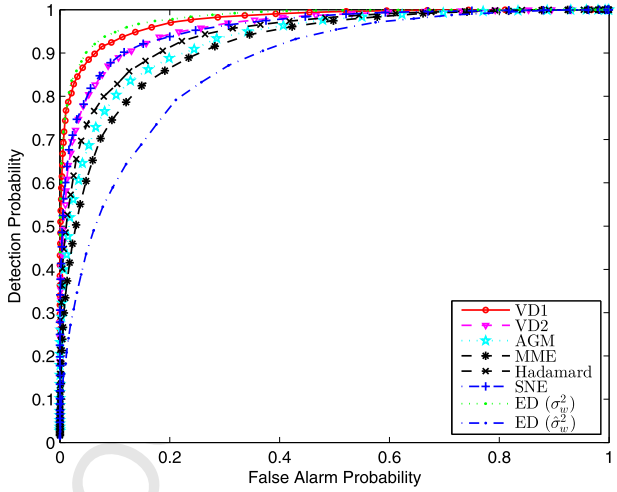

(a) Uniform noise.

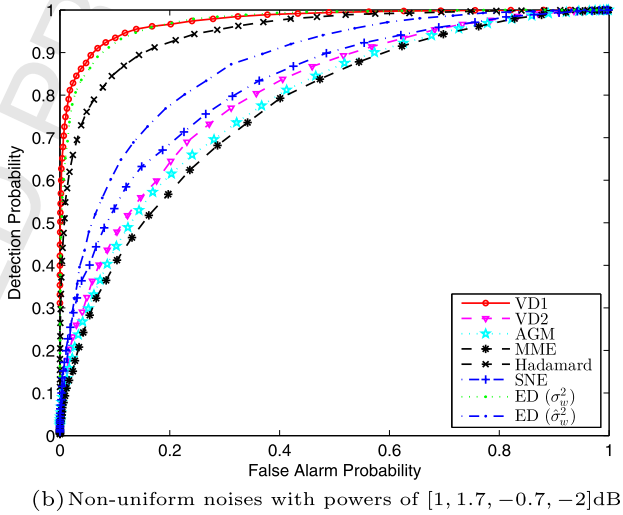

(b) Non-uniform noises with powers of $[1, 1.7, -0.7, -2]$dB.

Fig. 4. ROCs of various detectors for QPSK signals in Rayleigh-fading channel. $m = 4$, $n = 30$, $d = 1$ and SNR $= -5$ dB.

close to each other in this case. The Hadamard ratio detector has the similar behavior as the AGM and MME methods but all of them are inferior to the former four schemes. However, the ED($\hat{\sigma}_w^2$) detector has a big gap to the other methods, indicating that it is not an appropriate candidate for the large sample case. The empirical results for the non-uniform noise are illustrated in Fig. 5(b) where the noise powers are set as $[0, -1, 1.5, -0.8, 2, -1.7]$ dB. Again, only the robust detectors, i.e., the VD1 and Hadamard ratio methods, are able to keep their detection accuracy whereas other detectors, i.e., the VD2, AGM, MME, SNE and ED($\hat{\sigma}_w^2$) schemes, suffer from performance degradation.

The computational times for various algorithms are depicted in Fig. 6, where the eigenvalue-based methods use the MATLAB built-in function `SVD` and the proposed volume-based and Hadamard ratio approaches employ the MATLAB built-in function `det`. It is observed that, when the number of antennas is less than 15, all the methods have similar computational requirement. The VD2 detector is somewhat more computationally intensive than the VD1 scheme because additional computations are involved to estimate σ_w^2 and b. As the number of antennas becomes larger, however, the proposed VD1 approach requires much less computational cost than the eigenvalue-based detectors. Although the Hadamard ratio and ED($\hat{\sigma}_w^2$) schemes are more computationally efficient than the VD1 method, they provide inferior detection performance.

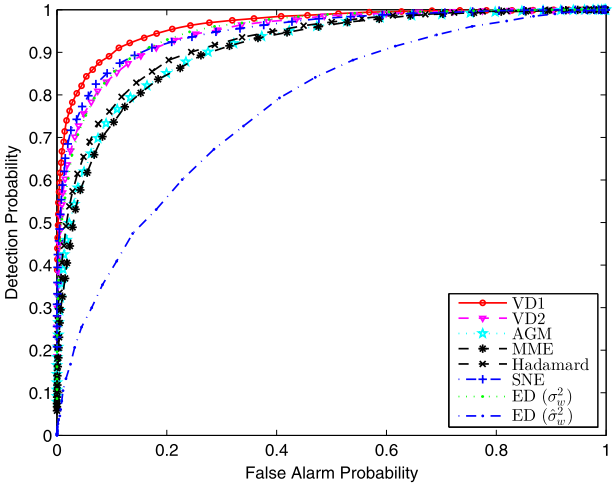

(a) Uniform noise.

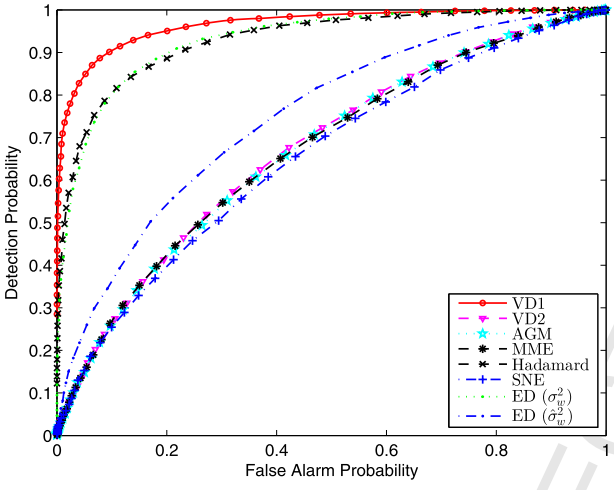

(b) Non-uniform noises with powers of $[0, -1, 1.5, -0.8, 2, -1.7]$dB.

Fig. 5. ROCs of various detectors for QPSK signals in Rayleigh-fading channel. $m = 6$, $n = 100$, $d = 1$ and SNR $= -10$ dB.

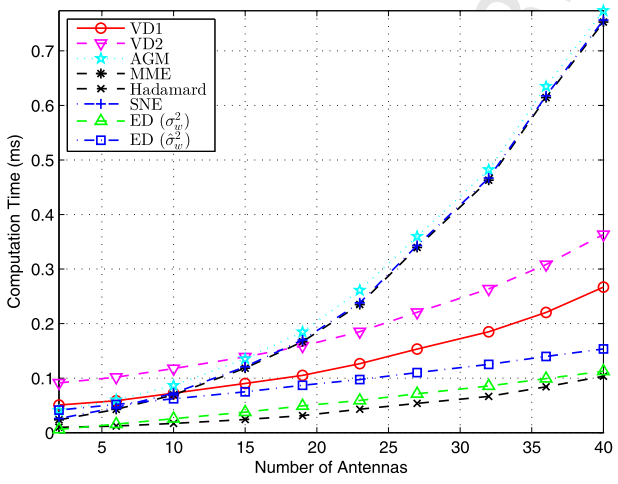

Fig. 6. Computational time versus number of antennas at $m/n = 0.6$.

5. Conclusion

The volume-based methods have been proposed for spectrum sensing. The distribution of the determinant of SCM, namely, the volume, can be accurately determined in the framework of RMT, which turns out to be a simple Gaussian distribution. Therefore, the theoretical threshold of the VD2 method is accurately determined by utilizing this distribution, particularly for the case when the number of samples and number of antennas are large and close to each other. Numerical results agree well with the theoretical analysis. For the VD1 method, however, its threshold cannot be theoretically calculated. Meanwhile, the theoretical detection probabilities of the VD1 and VD2 approaches cannot be computed yet. These will be tackled in our future works.

References

[1] Federal Communication Commission, Spectrum-policy task force, Rep. ET Docket, No. 02-135, Nov. 2002.
[2] J. Mitola III, Cognitive radio for flexible mobile multimedia communications, in: Proc. IEEE Mobile Multimedia Commun. Conf., San Diego, CA, USA, Nov. 1999, pp. 3–10.
[3] S. Haykin, Cognitive radio: Brain-empowered wireless communications, IEEE J. Sel. Areas Commun. 23 (2) (Feb. 2005) 201–220.
[4] G. Ganesan, Y. Li, Cooperative spectrum sensing in cognitive radio, Part I: Two user networks, IEEE Trans. Wirel. Commun. 6 (6) (Jun. 2007) 2204–2213.
[5] S. Haykin, D.J. Thomson, J.H. Reed, Spectrum sensing for cognitive radio, Proc. IEEE 97 (5) (May 2009) 849–877.
[6] A. Pérez-Neira, M. Lagunas, M. Rojas, P. Stoica, Correlation matching approach for spectrum sensing in open spectrum communications, IEEE Trans. Signal Process. 57 (12) (Dec. 2009) 4823–4836.
[7] V. Koivunen, S. Chaudhari, H.V. Poor, Autocorrelation-based decentralized sequential detection of OFDM signals in cognitive radios, IEEE Trans. Signal Process. 57 (7) (Jul. 2009) 2690–2700.
[8] A. Huttunen, J. Lundén, V. Koivunen, H.V. Poor, Collaborative cyclostationary spectrum sensing for cognitive radio systems, IEEE Trans. Signal Process. 57 (11) (Nov. 2009) 4182–4195.
[9] B.I. Ahmad, A. Tarczynski, Reliable wideband multichannel spectrum sensing using randomized sampling schemes, Signal Process. 90 (7) (Jul. 2010) 2232–2242.
[10] F.-X. Socheleaua, S. Houckea, P. Ciblatb, A. Aïssa-El-Beya, Cognitive OFDM system detection using pilot tones second and third-order cyclostationarity, Signal Process. 91 (2) (Feb. 2011) 252–268.
[11] B. Seo, Precoder design in cognitive radio networks with channel covariance information, Signal Process. 92 (12) (Dec. 2012) 3056–3061.
[12] Z. Quan, S. Cui, A.H. Sayed, H.V. Poor, Optimal multiband joint detection for spectrum sensing in cognitive radio networks, IEEE Trans. Signal Process. 57 (3) (Mar. 2009) 1128–1140.
[13] F.F. Digham, M.S. Alouini, M.K. Simon, On the energy detection of unknown signals over fading channels, IEEE Trans. Commun. 55 (1) (Jan. 2007) 21–24.
[14] S.V. Nagaraj, Entropy-based spectrum sensing in cognitive radio, Signal Process. 89 (2) (Feb. 2009) 174–180.
[15] Y. Zhuan, G. Memik, J. Grosspietsch, Energy detection using estimated noise variance for spectrum sensing in cognitive radio networks, in: Proc. IEEE Wireless Communications and Networking Conference (WCNC), Las Vegas, NV, Mar. 2008, pp. 711–716.
[16] B. Shen, L. Huang, C. Zhao, Z. Zhou, K. Kwak, Energy detection based spectrum sensing for cognitive radios in noise of uncertain power, in: Proc. International Symposium on Communications and Information Technologies (ISCIT), Oct. 2008, pp. 628–633.
[17] Y.M. Kim, G. Zheng, S.H. Sohn, J.M. Kim, An alternative energy detection using sliding window for cognitive radio system, in: Proc. International Conference on Advanced Communication Technology (ICACT), vol. 1, Gangwon-Do, Feb. 2008, pp. 481–485.
[18] T.J. Lim, R. Zhang, Y.-C. Liang, Y. Zeng, GLRT-based spectrum sensing for cognitive radio, in: Proc. IEEE Global Commun. Conf. (GLOBECOM), New Orleans, LO, Nov. 2008, pp. 1–5.
[19] Y. Zeng, Y.-C. Liang, Eigenvalue-based spectrum sensing algorithms for cognitive radio, IEEE Trans. Commun. 57 (6) (Jun. 2009) 1784–1793.
[20] A. Kortun, T. Ratnarajah, M. Sellathurai, C. Zhong, C.B. Papadias, On the performance of eigenvalue-based cooperative spectrum sensing for cognitive ratio, IEEE J. Sel. Top. Signal Process. 5 (1) (Feb. 2011) 49–55.
[21] A. Taherpour, M. Nasiri-Kenari, S. Gazor, Multiple antenna spectrum sensing in cognitive radios, IEEE Trans. Wirel. Commun. 9 (2) (Nov. 2010) 814–823.
[22] B. Nadler, F. Penna, R. Garello, Performance of eigenvale-based signal detectors with known and unknown noise level, in: Proc. IEEE International Conference on Communications (ICC), Kyoto, Japan, Jun. 2011, pp. 1–5.
[23] F. Penna, R. Garello, M. Spirito, Cooperative spectrum sensing based on the limiting eigenvalue ratio distribution in Wishart matrices, IEEE Commun. Lett. 13 (7) (Jul. 2009) 507–509.
[24] P. Wang, J. Fang, N. Han, H. Li, Multiantenna-assisted spectrum sensing for cognitive radio, IEEE Trans. Veh. Technol. 59 (4) (May 2010) 1791–1800.

[25] L. Wei, O. Tirkkonen, Spectrum sensing in the presence of multiple primary users, IEEE Trans. Commun. 60 (5) (May 2012) 1268–1277.
[26] C.A. Tracy, H. Widom, On orthogonal and symplectic matrix ensembles, Commun. Math. Phys. 177 (1996) 727–754.
[27] D. Ramírez, G. Vazquez-Vilar, R. López-Valcarce, J. Vía, I. Santamaría, Detection of rank-p signals in cognitive radio networks with uncalibrated multiple antennas, IEEE Trans. Signal Process. 59 (8) (Aug. 2011) 3764–3774.
[28] J.K. Tugnait, On multiple antenna spectrum sensing under noise variance uncertainty and flat fading, IEEE Trans. Signal Process. 60 (4) (Apr. 2012) 1823–1832.
[29] A. Mariani, A. Giorgetti, M. Chiani, Test of independence for cooperative spectrum sensing with uncalibrated receivers, in: Proc. of IEEE Global Communications Conference (GLOBECOM), Anaheim, CA, 3-7 Dec. 2012, pp. 1374–1379.
[30] R. López-Valcarce, G. Vazquez-Vilar, J. Sala, Multiantenna spectrum sensing for cognitive radio: Overcoming noise uncertainty, in: Proc. 2nd International Workshop on Cognitive Information Processing (CIP), Elba, 14–16 June, 2010, pp. 310–315.
[31] D. Ramírez, J. Vía, I. Santamaría, The locally most powerful test for multiantenna spectrum sensing with uncalibrated receivers, in: Proc. IEEE International Conference on Acoustics, Speech and Signal Processing (ICASSP), Kyoto, Japan, March 2012, pp. 3437–3440.
[32] A. Leshem, A.-J. van der Veen, Multichannel detection of Gaussian signals with uncalibrated receivers, IEEE Signal Process. Lett. 8 (April 2001) 120–122.
[33] Y. Chen, A. Wiesel, Y.C. Eldar, A.O. Hero, Shrinkage algorithms for MMSE covariance estimation, IEEE Trans. Signal Process. 58 (10) (Oct. 2010) 5016–5029.
[34] N. Giri, On the complex analysis of T^2- and R^2-tests, Ann. Math. Stat. 36 (1965) 665–670.
[35] B.T. Porteous, Improved likelihood ratio statistics for covariance selection models, Biometrika 72 (1985) 97–101.
[36] D. Jonsson, Some limit theorems for the eigenvalues of a sample covariance matrix, J. Multivar. Anal. 12 (1982) 1–38.
[37] Z.D. Bai, J.W. Silverstein, CLT for linear spectral statistics of a large dimensional sample covariance matrix, Ann. Probab. 32 (2004) 553–605.
[38] Q.T. Zhang, Advanced detection techniques for cognitive radio, in: Proc. IEEE International Conference on Communications (ICC), Dresden, Germany, Jun. 2009, pp. 1–5.
[39] Q.T. Zhang, Theoretical performance and thresholds of the multitaper method for spectrum sensing, IEEE Trans. Veh. Technol. 60 (5) (Jun. 2011) 2128–2138.
[40] M.D. Springer, Algebra of Random Variables, Wiley, New York, 1973.
[41] R.J. Muirhead, Aspects of Multivariate Statistical Theory, Wiley, New York, 1982.
[42] N.S. Alagha, Cramer-Rao bounds of SNR estimates for BPSK and QPSK modulated signals, IEEE Commun. Lett. 5 (1) (Jan. 2001) 10–12.
[43] J.-P. Delmas, H. Abeida, Cramer–Rao bounds of DOA estimates for BPSK and QPSK modulated signals, IEEE Trans. Signal Process. 54 (1) (Jan. 2006) 117–126.
[44] A. Abdi, J.A. Barger, M. Kaveh, A parametric model for the distribution of the angle of arrival and the associated correlation function and power spectrum at the mobile station, IEEE Trans. Veh. Technol. 51 (3) (May 2002) 425–434.
[45] A. Abdi, M. Kaveh, A space-time correlation model for multielement antenna systems in mobile fading channels, IEEE J. Sel. Areas Commun. 20 (Apr. 2002) 550–560.
[46] M. Chiani, M.Z. Win, A. Zanella, On the capacity of spatially correlated MIMO Rayleigh-fading channels, IEEE Trans. Inf. Theory 49 (10) (Oct. 2003) 2363–2371.

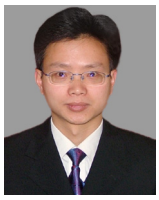

Lei Huang (M'07) was born in Guangdong, China. He received the B.Sc., M.Sc., and Ph.D. degrees in electronic engineering from Xidian University, Xi'an, China, in 2000, 2003, and 2005, respectively. From 2005 to 2006, he was a Research Associate with the Department of Electrical and Computer Engineering, Duke University, Durham, NC. From 2009 to 2010, he was a Research Fellow with the Department of Electronic Engineering, City University of Hong Kong and a Research Associate with the Department of Electronic Engineering, The Chinese University of Hong Kong. Since 2011, he has joined the Department of Electronic and Information Engineering, Harbin Institute of Technology Shenzhen Graduate School, where he is currently a Professor. His research interests include spectral estimation, array signal processing, statistical signal processing, and their applications in radar and wireless communication systems. He currently is an editorial board member of Digital Signal Processing.

Hing Cheung So (S'90–M'95–SM'07) was born in Hong Kong. He received the B.Eng. degree from the City University of Hong Kong and the Ph.D. degree from The Chinese University of Hong Kong, both in electronic engineering, in 1990 and 1995, respectively. From 1990 to 1991, he was an Electronic Engineer with the Research and Development Division, Everex Systems Engineering Ltd., Hong Kong. During 1995–1996, he worked as a Postdoctoral Fellow with The Chinese University of Hong Kong. From 1996 to 1999, he was a Research Assistant Professor with the Department of Electronic Engineering, City University of Hong Kong, where he is currently an Associate Professor. His research interests include statistical signal processing, fast and adaptive algorithms, signal detection, parameter estimation, and source localization. Dr. So has been on the editorial boards of the IEEE TRANSACTIONS ON SIGNAL PROCESSING, Signal Processing, Digital Signal Processing, and ISRN Applied Mathematics, as well as a member of the Signal Processing Theory and Methods Technical Committee of the IEEE Signal Processing Society.

Cheng Qian was born in China on November 27, 1988. He received the B.E. degree in communication engineering from Hangzhou Dianzi University, Hangzhou, China, in 2011, and M.E. degree in communication and information engineering from Harbin Institute of Technology (HIT), Shenzhen, China, in 2013. He is currently pursuing the Ph.D degree in the field of communication and information engineering at HIT. His research interests are in array signal processing and MIMO radar.